AIAA JOURNAL
Vol. 34, No. 2, February 1996

Modeling Nonaxisymmetric Off-Design Shapes of Large Scientific Balloons

Frank Baginski*
George Washington University, Washington, D.C. 20052

The design of a large scientific balloon is usually based on an axisymmetric model, describing its shape at float altitude. However, the shapes observed during ascent are clearly nonaxisymmetric and are characterized by a number of distinctive features, including a periodic lobe pattern surrounding the gas bubble, internally folded balloon fabric, and flat winglike structures in the lower portion of the balloon below the gas bubble. In this paper, we present a mathematical model that captures the complex geometries of these off-design shapes. Real balloons are made from long tapered sheets of polyethylene that are sealed edge to edge. We base our geometric model on this construction, enabling us to define a reference configuration and to estimate the distortion in our computed balloon shapes. We compute one-parameter families of ascent shapes with triangular, square-shaped, and pentagonal symmetries. Our computed solutions possess many nonaxisymmetric features that are observed in real balloons.

Nomenclature

$\mathcal{C}_k$ = class of piecewise differentiable surfaces with D_k symmetry
$d(\cdot,\cdot)$ = measures the intrinsic distance between vertices lying on a common circumferential or meridional fiber
E = sum of the gravitational potential energies of the lifting gas and balloon film
$\mathcal{F}_{i,j}$ = internal fold of a subregion in a pseudogore
g = acceleration due to gravity
L_m = edge length of a pseudogore
$N_{\mathcal{T}}$ = number of facets in a triangulation of $\mathcal{S}_f$
n_c = number of circumferential fibers
P_{xz} = projection onto x–z plane, $P_{xz}[v] = (v_1, 0, v_3)$ where $v = (v_1, v_2, v_3)$
P_z = projection onto z axis, $P_z[v] = (0, 0, v_3)$ where $v = (v_1, v_2, v_3)$
$\mathcal{P}_{\text{hook}}$ = hook plane, $\{(x, y, z) \in R^3 \mid y = 0\}$
$\mathcal{P}_{\text{wing}}$ = wing plane, $\{(x, y, z) \in R^3 \mid y = \tan(\pi/k)x\}$, where k corresponds to D_k
$\mathcal{Q}_{i,j}$ = subregion of a pseudogore
$R(s)$, $Z(s)$ = generating curve for the float shape where s is arclength
$r_{\max}$ = $\max\{(x_{i,j}^2 + y_{i,j}^2)^{1/2}, i = 1, \ldots, n_c + 1, j = 1, \ldots, 2p + 2\}$ where $v_{i,j} = (x_{i,j}, y_{i,j}, z_{i,j})$ is a vertex in $\mathcal{S}(v_{i,j})$
$\mathcal{S}$ = balloon surface
$\mathcal{S}_f(v_{i,j})$ = fundamental section of a balloon shape defined by the set of vertices $\{v_{i,j}\}$
$\mathcal{S}_f$ = fundamental section of an asymmetric ascent shape
$\mathcal{S}_f'$ = reflection of $\mathcal{S}_f$ in the $y = 0$ plane
$\mathcal{T}_l$ = facet in an approximation of $\mathcal{S}_f$
$V_{i,j}^L$ = ith vertex on the left edge of the jth gore in the reference configuration
$V_{i,j}^M$ = $(V_{i,j}^L + V_{i,j}^R)/2$
$V_{i,j}^R$ = ith vertex on the right edge of the jth gore in the reference configuration
$\mathcal{V}$ = gas volume of balloon surface $\mathcal{S}$
$\mathcal{V}_{\text{float}}$ = gas volume at float altitude
$\mathcal{V}_l$ = volume of tetrahedron formed by joining vertices of $\mathcal{T}_l$ to a base point on z axis inside gas bubble
$v_{i,j}^L$ = ith vertex on the left edge of the jth gore in the balloon shape
$v_{i,j}^R$ = ith vertex on the right edge of the jth gore in the balloon shape
$|v|$ = $\sqrt{(v_1^2 + v_2^2 + v_3^2)}$ where $v = (v_1, v_2, v_3)$
$\mathcal{W}^k$ = $(\{x, y, z) \in R^3 \mid 0 \le y \le \tan(\pi/k)x\}$
$z_{\max}$ = balloon height (measured from tail to apex)
μ = constant, proportional to $g \cdot \rho_{\text{film}}$
ρ = constant for a fixed altitude, $g(\rho_{\text{gas}} - \rho_{\text{air}})$
ρ_{air} = density of ambient air, mass per unit volume
ρ_{film} = balloon film density, mass per unit area
ρ_{gas} = density of the lifting gas, mass per unit volume

I. Introduction

DURING ascent to float altitude, a large scientific balloon is observed to have a number of distinctive features, which include 1) a spherical top, 2) a periodic lobe pattern surrounding the gas bubble, 3) internally folded balloon fabric, and 4) flat winglike structures below the gas bubble. To increase the performance of current balloon technology or aid in the analysis of new balloon designs, it would be desirable to estimate the stresses and strains for a balloon shape with features 1–4. However, before this task can be undertaken, an accurate geometric model capable of handling the nonstandard geometries of ascent shapes is needed. Because the features of ascent shapes differ radically from the axisymmetric design shape, they are sometimes referred to as off-design shapes.

The standard model for a balloon shape is a system of nonlinear ordinary differential equations developed by researchers at the University of Minnesota.[1] In this model, one typically assumes that the circumferential stress is zero and all tension is carried in the meridional direction. The solutions generate surfaces of revolution (called Σ shapes) that are used in determining the design (float) shape. Since the Σ shapes are axisymmetric, they are not able to handle features 2–4. An approach to computing nonaxisymmetric ascent shapes based on a variational principle was presented in Ref. 3. These shapes were called energy-minimizing shapes (or EM shapes) and possessed features 1–4. However, the model in Ref. 3 gave only a crude description of internally folded material.

To improve the aspects of the model in Ref. 3 that pertain to the distribution of excess balloon fabric, one needs to look at the construction of a real balloon. A real balloon is made from long flat tapered sheets of polyethylene called gores that are sealed edge to edge. This gore structure is important in modeling partially inflated balloon shapes because internal folds tend to form along the center

Received Oct. 31, 1994; revision received April 7, 1995; accepted for publication April 11, 1995.

*Associate Professor, Department of Mathematics. Member AIAA.

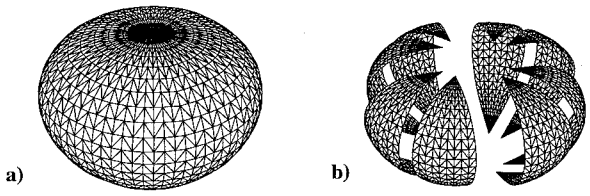

Fig. 1 a) Float shape $\mathcal{S}_{\text{float}}$ and b) $\mathcal{S}_{\text{float}}$ partitioned into fundamental sections.

of these structures. The gore structure was not represented in the model in Ref. 3, and all excess material was assumed to lie in one of the hook planes. In addition, because there was no well-defined reference configuration, it was not possible to measure the distortion in a computed shape. In the work presented here, we improve the way in which internally folded material is modeled and introduce a reference configuration related to the gore structure. Although we model the balloon as a deformable structure, it is not treated as a membrane in the classical sense. We first outline some terminology that will be used throughout the paper.

The lobe pattern surrounding the gas bubble of a real ascent shape motivates us to consider shapes with dihedral symmetry. The dihedral group D_k is the group of motions of the plane generated by rotations about the origin through an angle of $2\pi/k$ and reflections about some fixed axis. A shape with D_k symmetry has the same symmetries as a regular polygon with k sides. For example, if we look down onto the top of a balloon shape with three lobes, we would observe a pattern with triangular symmetry and we would say that the shape has D_3 symmetry (see Sec. VI). This leads us to a geometric construction of a balloon shape, based on the symmetry group D_k. In Ref. 3, the basic building block was the fundamental section $\mathcal{S}_f$, which was assumed to lie inside the wedge $\mathcal{W}^k = \{(x, y, z) \in R^3 \mid 0 \le y \le \tan(\pi/k)x\}$. The boundary of $\mathcal{S}_f$ is formed by two planar curves called the hook and wing profiles, respectively. The hook profile of $\mathcal{S}_f$ is situated in the plane $y = 0$ (denoted by $\mathcal{P}_{\text{hook}}$), and its wing profile lies in the plane $y = \tan(\pi/k)x$ (denoted by $\mathcal{P}_{\text{wing}}$). The term $\mathcal{S}'_f$ is obtained by reflecting $\mathcal{S}_f$ in $\mathcal{P}_{\text{hook}}$. The complete shape is assembled from k copies of $\mathcal{S}_f \cup \mathcal{S}'_f$ using the symmetries of D_k (see Refs. 2 and 3 for further details on this construction). The class of balloon shapes with dihedral symmetry D_k will be denoted by $\mathcal{C}_k$, and $\mathcal{S}$ will denote a complete shape in $\mathcal{C}_k$. A typical float shape is shown in Fig. 1a. A float shape partitioned into four fundamental sections and four mirror images is shown in Fig. 1b.

In an actual balloon, load tapes are attached along the edges of gores and end fittings are located at the top and bottom of the balloon. These features are not included in our model. Depending on design parameters, there may be as many as 180 gores in a real balloon. From a practical standpoint, it is not feasible to include every gore in a numerical model, and for this reason, we introduce a structure called a pseudogore (see Ref. 2). Roughly speaking, a pseudogore is obtained by cutting the design shape along N_g equally spaced meridians (see Fig. 1) and flattening each into a plane. The properties of a pseudogore are discussed in Sec. II.

In the work presented here, the basic building block is the pseudogore. The fundamental section $\mathcal{S}_f$ is subdivided into p pseudogores plus the right half of one pseudogore (because material is folded in the $y = 0$ plane, continuity of the complete shape requires that a half-pseudo-gore is needed in each fundamental section). In Fig. 2, we have decomposed the fundamental section of a balloon shape into four and one-half pseudogores, flattening each into a plane (the pseudogores presented in Fig. 2 have been scaled for display purposes). The triangulation of a pseudogore is discussed in Sec. II. We refer to the flattened pseudogore as the reference configuration. A fundamental section in a partially inflated balloon shape is constructed from $p + 1/2$ deformed pseudogores. Each pseudogore could include an internal fold, if excess material is present. See Fig. 3 for an interior view of a typical fundamental section showing the internal folds.

In our model, the complete faceted balloon surface has $N_g = 2k \times (p+1/2)$ pseudogores. We assume that the generating curve for the float shape, $(R(s), Z(s))$, $0 \le s \le L_m$, and design parameters

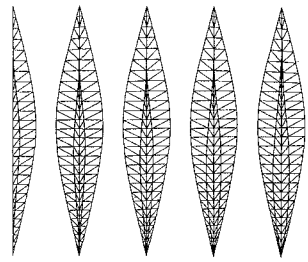

Fig. 2 $\mathcal{S}_f$ decomposed into pseudogores and triangulated.

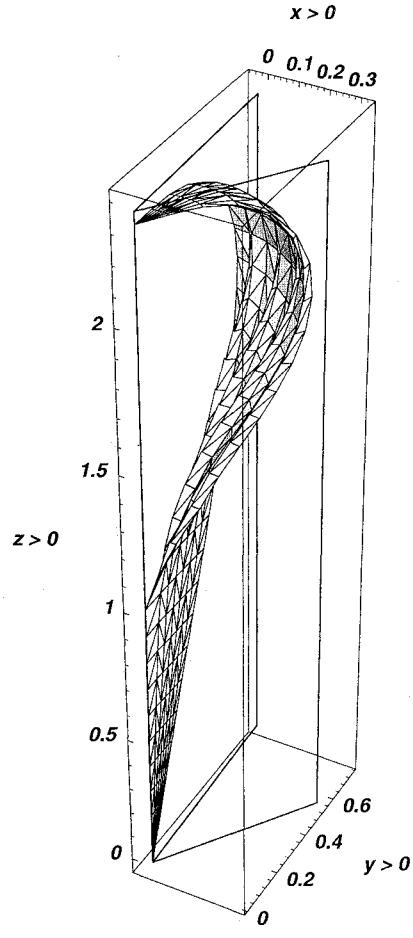

Fig. 3 Inside view of $\mathcal{S}_f$ showing internal folds.

are known. The gore width s units from the base of the balloon is $H(s) = 2\pi R(s)/N_g$ (see Fig. 4). When the volume of $\mathcal{S}$ is less than what it would be at float, a shape with D_k symmetry will have k lobes and k wing sections. Each lobe is centered over a wing section. All balloon fabric below the gas bubble lies in a wing plane. Running along the center of each pseudogore is an internal fold of excess material (see Fig. 3).

A family of off-design EM shapes is a sequence $(\mathcal{V}^i, \mathcal{S}^i)$, $i = 0, 1, \ldots, n$, where $\mathcal{V}^i$ is the volume of the gas bubble, $\mathcal{V}^0 < \mathcal{V}^1 < \cdots < \mathcal{V}^n \le \mathcal{V}_{\text{float}}$, and $\mathcal{S}^i$ is a balloon shape in $\mathcal{C}_k$ for some fixed k. To determine a family of ascent shapes, we begin by computing $\mathcal{S}^0$ with an initial guess that is based on the profile curves in Ref. 4. The initial guess is evolved to equilibrium, and then $\mathcal{S}^0$ is used to compute an initial approximation for $(\mathcal{V}^1, \mathcal{S}^1)$. The process is repeated to generate the entire family. We found that the models presented in Refs. 2 and 3 were inadequate for computing families of ascent shapes over a large range of volumes. Errors accumulated in computing $\mathcal{S}^0, \mathcal{S}^1, \ldots, \mathcal{S}^i$ are passed on to the $i+1$ step. Eventually, these errors become large relative to the lengths of certain fiber segments. The net effect is that certain constraints cannot be met and the solution process diverges. We were able to control the size of the constraint residuals by introducing a vertex-averaging scheme

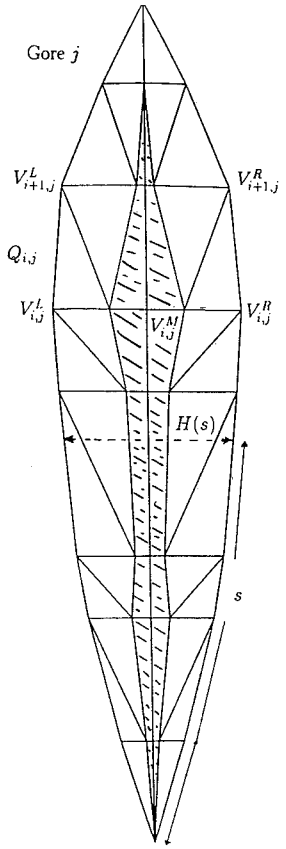

Fig. 4 Schematic of flat pseudogore.

into our formulation. The vertex-averaging scheme is discussed in Sec. V.

In Sec. III, we describe the boundary conditions that are applied to a shape in $\mathcal{C}_k$. The variational principle for an EM shape with pseudogores is presented in Sec. IV. In Sec. VI, we present EM shapes with triangular, square-shaped, and pentagonal symmetry. These symmetries were chosen to illustrate our methods, but shapes with other symmetries can also be computed. In Sec. VII, we discuss the distortion in our computed EM shapes. Section VIII contains some concluding remarks.

II. Pseudogore Element

In this section, we outline the relation between a pseudogore in $\mathcal{S}$ and its reference configuration. First, we define some notation (refer to Figs. 4 and 5). The reference configuration lies in the u–v plane with its tail at the origin. The edge from $V^L_{i,j}$ to $V^R_{i,j}$ is $E_{i,j} = V^R_{i,j} - V^L_{i,j}$ and its length is $|E_{i,j}|$ where $|\cdot|$ is Euclidean distance. For convenience, we define $V^L_{i,1} = (-u^R_{i,1}, v^R_{i,1})$ where $V^R_{i,1} = (u^R_{i,1}, v^R_{i,1})$.

Lower case letters refer to vertices and edges in $\mathcal{S}$. The terms $v^L_{i,j}$ and $v^R_{i,j}$ are identified with $V^L_{i,j}$ and $V^R_{i,j}$, respectively. By construction, $v^R_{i,j} = v^L_{i,j+1}$ and $v^M_{i,j} = (v^L_{i,j} + v^R_{i,j})/2$. The vertices $v^M_{i,1}$ are determined from boundary conditions (see Sec. III).

A fiber of length at least $|E_{i,j}|$ connects $v^L_{i,j}$ to $v^R_{i,j}$. Its intrinsic length is

$$d\left(v^L_{i,j}, v^R_{i,j}\right) = \left|v^L_{i,j} - v^M_{i,j}\right| + \left|v^R_{i,j} - v^M_{i,j}\right| + 2|f_{i,j}| \tag{1}$$

where the length of the internally folded fiber segment is $2|f_{i,j}|$ and

$$|f_{i,j}| = \tfrac{1}{2}\max\left\{0, |E_{i,j}| - d\left(v^L_{i,j}, v^R_{i,j}\right)\right\} \tag{2}$$

If $v^L_{i,j}$, $v^M_{i,j}$, and $v^R_{i,j}$ are collinear, Eq. (1) can be simplified. However, after vertex averaging (see Sec. V), $v^L_{i,j}$, $v^M_{i,j}$, and $v^R_{i,j}$ need not be collinear. During the computation of an EM shape, $d(v^L_{i,j}, v^R_{i,j})$ may exceed $|E_{i,j}|$. In this case, $|f_{i,j}| = 0$ and the corresponding fiber

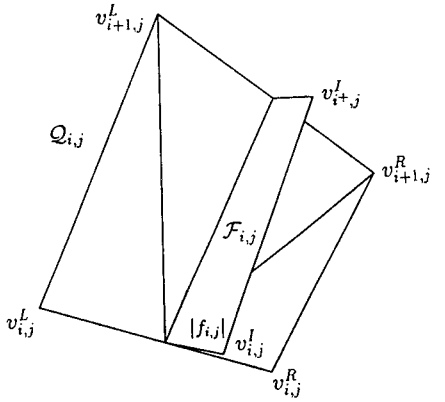

Fig. 5 $\mathcal{Q}_{i,j} \cup \mathcal{F}_{i,j}$ where $\mathcal{F}_{i,j}$ is folded material.

segment is stretched. We define $f_{i,j}$ to be the inward normal vector to $\mathcal{S}_f$ at $v^M_{i,j}$ with length $|f_{i,j}|$ (see Fig. 5) and

$$v^I_{i,j} = v^M_{i,j} + f_{i,j} \tag{3}$$

$$v^I_{i+,j} = v^M_{i+1,j} + \frac{|f_{i+1,j}|}{|f_{i,j}|} f_{i,j} \tag{4}$$

Vertices $v^I_{i,j}$, $v^M_{i,j}$, $v^M_{i+1,j}$, and $v^I_{i+,j}$ are joined to form facets of folded material $\mathcal{F}_{i,j}$ and the various $\mathcal{F}_{i,j}$ are triangulated. While $v^I_{i,j}$ and $v^I_{i+,j}$ are defined in Eqs. (3) and (4) for all i, below the gas bubble, the excess material is folded back into $\mathcal{P}_{\text{wing}}$. The various $\mathcal{Q}_{i,j}$ form the "exterior" of the balloon shape. The fabric in $\mathcal{Q}_{i,j}$ may also be wrinkled or stretched in some (unknown) fashion. During the evolution of an EM shape, the subregion $R_{i,j} = Q_{i,j} \cup F_{i,j}$ is always identified with $\mathcal{R}_{i,j} = \mathcal{Q}_{i,j} \cup \mathcal{F}_{i,j}$. The shaded region in Fig. 4 is roughly the pre-image of the folded material in the jth gore. In practice, the edges $\{E_{i,j}, i = 2, \ldots, n_c+1\}$ need not be parallel (see, for example, Fig. 2). Figure 3 shows an inside view of a fundamental section with four and one-half pseudogores.

The faceted surface approximating the fundamental section will be denoted by $\mathcal{S}_f$, i.e.,

$$\mathcal{S}_f = \bigcup_{(i,j)\in\mathcal{J}} \mathcal{R}_{i,j}, \qquad \mathcal{J} = \{(i,j) \mid 1 \le i \le n_c+1,\ 1 \le j \le p+1\}$$

The facets in $\mathcal{S}_f$ are formed using the vertices in $\{v^R_{i,j}, v^M_{i,j}, v^I_{i,j}, v^I_{i+,j} \mid (i,j) \in \mathcal{J}\}$. The various $v^R_{i,j}$ are independent (subject to boundary conditions); $v^M_{i,j}$, $v^I_{i,j}$, and $v^I_{i+,j}$ are computed from the various $v^R_{i,j}$.

When measuring distances in the EM shape, it will be useful to have a notation that does not depend on the superscripts L, M, and R. For this reason, we define

$$v_{i,2j-1} = v^M_{i,j}, \qquad \text{for} \quad j = 1, \ldots, p+1 \tag{5}$$

$$v_{i,2j} = v^R_{i,j}, \qquad \text{for} \quad j = 1, \ldots, p+1 \tag{6}$$

By definition, $v_{1,j} = v_{1,1}$ and $v_{n_c+2,j} = v_{n_c+2,1}$ for all j. To indicate that $\mathcal{S}_f$ is a function of the vertices, we will write $\mathcal{S}_f(v_{i,j})$. The term $\mathcal{S}(v_{i,j})$ will denote a shape in $\mathcal{C}_k$ generated by $\mathcal{S}_f(v_{i,j})$.

We define the intrinsic distance between vertices on the jth meridian in the following way:

$$d(v_{i,j}, v_{i+l,j}) = \sum_{k=1}^{l-1} |v_{i+k,j} - v_{i+k-1,j}|, \qquad 1 \le j \le i+l \le n_c+2$$

The intrinsic distance between vertices on the edges of the jth pseudogore is given by

$$d(v_{i,2j}, v_{i,2j+2}) = |v_{i,2j} - v_{i,2j+1}| + |v_{i,2j+1} - v_{i,2j+2}| + 2|f_{i,j}|$$

A meridional fiber in $\mathcal{S}_f(v_{i,j})$ is identified with its corresponding edge in the reference configuration. Vertices in $\mathcal{S}_f(v_{i,j})$ can move, but the total length of a meridional fiber in the final solution must

equal the length of the corresponding fiber in the reference configuration. Fibers that form edges where an internal fold initiates are not constrained. We allow the circumferential fiber segments to stretch, although we find there is little stretching of this type (see Sec. VII). Because the distance between adjacent vertices on a meridian may change, the length of a circumferential reference fiber will depend on the current set of vertices.

III. Boundary Conditions

In real balloons, circumferential fibers above the gas bubble appear to meet $\mathcal{P}_{\text{hook}}$ orthogonally (see Ref. 5). Near (but slightly above) the base of the gas bubble, these fibers need not be normal to $\mathcal{P}_{\text{hook}}$. Below the gas bubble, the fabric meets the central axis of the balloon shape (the z axis) in a rather complicated way, and we will make some crude assumptions to model this region. Below the gas bubble, all balloon fabric lies in the wing planes. Next, we outline the boundary conditions for the wing and hook profiles of a shape in $\mathcal{C}_k$.

The x and z coordinates of $v_{i,2p+2} \in \mathcal{P}_{\text{wing}}$ are independent. For a shape in $\mathcal{C}_k$, we find

$$v_{i,2p+2} = (x_{i,2p+2}, \tan(\pi/k)x_{i,2p+2}, z_{i,2p+2}) \quad \text{for} \quad v_{i,2p+2} \in \mathcal{P}_{\text{wing}} \tag{7}$$

By definition, $v_{i,1} = (x_{i,1}, y_{i,1}, z_{i,1}) \in \mathcal{P}_{\text{hook}}$ and $v_{i,2} = (x_{i,2}, y_{i,2}, z_{i,2})$ are vertices on the adjacent meridional fiber. In this case, we define

$$v_{i,1} = \begin{cases} P_{xz}[v_{i,2}] & \text{if} \quad v_{i,2} \notin \mathcal{P}_{\text{wing}} \\ P_z[v_{i,2}] & \text{if} \quad v_{i,2} \in \mathcal{P}_{\text{wing}} \end{cases} \tag{8}$$

IV. Problem Formulation

As in Ref. 3, we define the total energy E of a balloon configuration as

$$E = \rho \int_v z \, \mathrm{d}V + \mu \int_S z \, \mathrm{d}S \tag{9}$$

where the first integral is the gravitational potential energy of the lifting gas and the second integral is the gravitational potential energy of the balloon fabric. The term $\rho < 0$ is a constant proportional to the difference between the densities of the lifting gas and ambient air; μ is proportional to the film density.

For $\mathcal{S}_f(v_{i,j}) \subset \mathcal{W}^k$, the energy $E(v_{i,j})$ is (see Ref. 2)

$$E(v_{i,j}) = \rho \sum_{l=1}^{N_\mathcal{T}} \int_{\mathcal{T}_l} \frac{1}{2} z^2 \boldsymbol{k} \cdot \mathrm{d}\boldsymbol{A} + \mu \sum_{l=1}^{N_\mathcal{T}} \omega(\mathcal{T}_l) \int_{\mathcal{T}_l} z \, \mathrm{d}A \tag{10}$$

where $\mathcal{S}_f(v_{i,j}) = \cup_{l=1}^{N_\mathcal{T}} \mathcal{T}_l$ and $\{\mathcal{T}_l, l = 1, \ldots, N_\mathcal{T}\}$ is a triangulation of $\mathcal{S}_f(v_{i,j})$ (see Ref. 6 for other problems involving surfaces determined by variational principles). Each $\mathcal{T}_l$ lies in exactly one $\mathcal{R}_{i,j}$, and so we can define

$$\omega(\mathcal{T}_l) = m(R_{i,j})/m(\mathcal{R}_{i,j}), \quad \text{if} \quad \mathcal{T}_l \in \mathcal{R}_{i,j} \quad i = 1, \ldots, n_c + 1, \; j = 1, \ldots, p + 1$$

where $m(\mathcal{A})$ denotes the sum of the areas of the triangles in $\mathcal{A}$ [in Ref. 3, the total surface area was a constraint and $\omega(\mathcal{T}_l) = 1$ for all l]. In practice, we found that $m(\mathcal{R}_{i,j}) > 0$. The definition of $\omega(\cdot)$ ensures that the mass of $R_{i,j}$ equals the mass of $\mathcal{R}_{i,j}$. The constraints are

$$\mathcal{V} - 2k \sum_{l=1}^{N_\mathcal{T}} \mathcal{V}_l = 0 \tag{11}$$

$$L_m - d\left(v_{1,2j}, v_{n_c+2,2j}\right) = 0, \qquad j = 1, \ldots, p + 1 \tag{12}$$

$$|v_{i,1} - v_{i,2}| - \tfrac{1}{2}|E_{i,1}| \le 0, \qquad i = 2, \ldots, n_c + 1 \tag{13}$$

$$\sum_{k=0}^{1} |v_{i,2j+k} - v_{i,2j+k+1}| - |E_{i,j}| \le 0 \quad i = 2, \ldots, n_c + 1, \quad j = 2, \ldots, p + 1 \tag{14}$$

where $\mathcal{V}_l$ is the volume of the lth tetrahedron in a partition of the gas bubble. Upper and lower bounds on the vertices in the form

$$v_{i,2j}^{lb} \le v_{i,2j} \le v_{i,2j}^{ub}, \qquad 2 \le i \le n_c + 2, \qquad 1 \le j \le p + 1 \tag{15}$$

are included. The vector inequalities in Eq. (15) are interpreted component-wise.

We are led to the following variational principle: For $\mathcal{S}(v_{i,j}) \in \mathcal{C}_k$, Problem ($\star$),

Minimize

$$E(v_{i,j})$$

subject to

$$\boldsymbol{G}(v_{i,j}) = 0$$

$$\boldsymbol{J}(v_{i,j}) \le 0$$

satisfying Eq. (15), where $\boldsymbol{G}$ is defined by the left side of Eqs. (11) and (12) and $\boldsymbol{J}$ is defined by the left side of Eqs. (13) and (14). A solution of Problem ($\star$) is called an energy-minimizing or EM shape. We used Matlab software constr to compute numerical solutions of Problem ($\star$) (see Sec. VII); constr uses a sequential quadratic programming method by Powell.[7]

V. Vertex Averaging

The variational principle defined in Problem ($\star$) differs from Eqs. (1–4) of Ref. 2 in the way in which the circumferential fiber constraints are modeled. In Ref. 2, the total length of a circumferential fiber was required to be preserved. When trying to compute a family of ascent shapes, we found that the residual errors in these circumferential constraints grew with each successive EM shape that was computed. We were able to improve our results by replacing Eq. (4) of Ref. 2 with the inequalities (13) and (14) and allowing circumferential fiber segments to stretch. Our results were improved further by vertex averaging before evaluating the objective function and constraints. Formally, this is accomplished by replacing $\mathcal{S}_f(v_{i,j})$ with $\mathcal{S}_f(\hat{v}_{i,j})$, where $\hat{v}_{i,j}$ represents an average taken over the neighbors of $v_{i,j}$. In this section, we describe the averaging process. As defined in Sec. III, $v_{i,j}$ denotes a vertex that lies on the jth meridional fiber and the ith circumferential fiber. Vertices in the form $v_{i,j}^I$ or $v_{i+,j}^I$ are computed after vertex averaging has been completed.

The vertex at the tail of the balloon is fixed at the origin, i.e., $v_{1,j} = (0, 0, 0)$ for all j. The vertex at the apex is averaged in the following way:

$$\hat{v}_{n_c+2,1} = \frac{1}{2p+3} P_z \left[v_{n_c+2,1} + \sum_{j=1}^{2p+2} v_{n_c+1,j} \right] \tag{16}$$

and $v_{n_c+2,j} = v_{n_c+2,1}$ for all j. There are two other cases to consider. If $j = 1$ or $2p + 2$, then

$$\hat{v}_{i,j} = \tfrac{1}{3}(v_{i+1,j} + v_{i,j} + v_{i-1,j}), \qquad 2 \le i \le n_c + 1 \tag{17}$$

If $j \ne 1$ or $2p + 2$, then

$$\hat{v}_{i,j} = \tfrac{1}{5}(v_{i+1,j} + v_{i-1,j} + v_{i,j} + v_{i,j-1} + v_{i,j+1}) \qquad 2 \le i \le n_c + 1 \tag{18}$$

Note that $\hat{v}_{i,2j}$, $\hat{v}_{i,2j+1}$, and $\hat{v}_{i,2j+2}$ need not be collinear.

We found that our numerical results could be improved by iterating Eqs. (16–18). We begin by setting $\hat{v}_{i,j}^{(0)} = v_{i,j}$. The iteration scheme is defined by Eqs. (16–18) where we replace $\hat{v}_{i,j}$ with $\hat{v}_{i,j}^{(n)}$ and terms in the form $v_{i',j'}$ with terms in the form $v_{i',j'}^{(n-1)}$, respectively. For the results presented here, we set $n = 2$ and use $\mathcal{S}_f(\hat{v}_{i,j}^{(2)})$ to evaluate the energy and constraint functions. To simplify notation in the following sections, we will drop the "hat" and superscript notation and simply write $\mathcal{S}_f(v_{i,j})$ for the shape obtained after vertex averaging has been carried out.

VI. Families of EM Shapes

In the following section, we present numerical results on families of ascent shapes with triangular, square-shaped, and pentagonal

symmetries. The initial guess for an EM shape with target volume $\mathcal{V} = \mathcal{V}^{(i)}$ will be denoted by $\mathcal{S}_f^{(i)}$. The corresponding solution and computed volume are denoted by $\mathcal{S}_f^i$ and $\mathcal{V}^i$, respectively.

When generating a family, we began with a volume $\mathcal{V}^{(0)} = 0.56278$. The term $\mathcal{S}_f^{(0)}$ was the ruled surface based on the Winker profiles (see Refs. 3 and 4). After $\mathcal{S}_f^0$ is computed, the volume was incremented in steps of size $\Delta\mathcal{V} = 0.115$ until the float volume is reached ($\mathcal{V}_{\text{float}} = 3.4$). Using the preceding notation, $\mathcal{V}^{(i)} = \mathcal{V}^{i-1} + \Delta\mathcal{V}$ for $1 \leq i \leq 25$. For $i \geq 1$, $\mathcal{S}_f^{(i)}$ was obtained by linear interpolating between $\mathcal{S}_f^{i-1}$ and the float shape. The approximate float shape was divided into N_g pseudogores and triangulated (see Table 1 for the values of p and N_g). The number of circumferential fibers was chosen to be $n_c = 22$.

In Figs. 6–8, we present EM shapes with triangular, square-shaped, and pentagonal symmetry for three different volumes. Unlike Fig. 3, the internally folded material in Figs. 6–8 is displayed separately from nonfolded facets for easier viewing.

At launch, the volume of the gas bubble is less than 1% of $\mathcal{V}_{\text{float}}$. We were able to compute families $(\mathcal{V}^i, \mathcal{S}^i)$ for $\mathcal{V}^i > \mathcal{V}^{i+1}$ with a volume as low as 5% of $\mathcal{V}_{\text{float}}$. To compute an EM shape with volume less than 5% of $\mathcal{V}_{\text{float}}$, one would need to generate a grid with a denser circumferential fiber spacing near the top of the balloon where the gas bubble is located.

VII. Measuring the Distortion in an EM Shape

By construction, every triangle $\mathcal{T}_l$ in an EM shape can be identified with a triangle $\mathcal{T}_l^R$ in the reference configuration. The mapping that takes $\mathcal{T}_l^R$ to $\mathcal{T}_l$ is defined implicitly by the solution process that evolves the EM shape. The mapping involves rigid-body displacements and in-plane displacements (stretches and contractions). To measure the distortion in an EM shape, one should ignore the rigid-body displacements and focus on the in-plane displacements. In the following, a typical facet $\mathcal{T}_l$ in a triangulation of $\mathcal{S}_f$ has three edges: $e_{m,l}$—a segment of a meridional fiber, $e_{c,l}$—a segment of a

Table 1 Extreme values of δ_m^+, δ_c^+, $\delta_d^\pm$, and $\hat{\delta}_d^\pm$ for families of EM shapes

Symmetry	k	p	N_g	δ_m^+	δ_c^+	δ_d^-	δ_d^+	$\hat{\delta}_d^-$	$\hat{\delta}_d^+$
Triangular	3	12	33	0.00189	0.04470	−0.06517	0.08857	−0.01542	0.02560
Square-shaped	4	10	36	0.00153	0.02700	−0.10618	0.13952	−0.02275	0.02840
Pentagonal	5	8	35	0.00174	0.01970	−0.16562	0.20386	−0.03688	0.03554

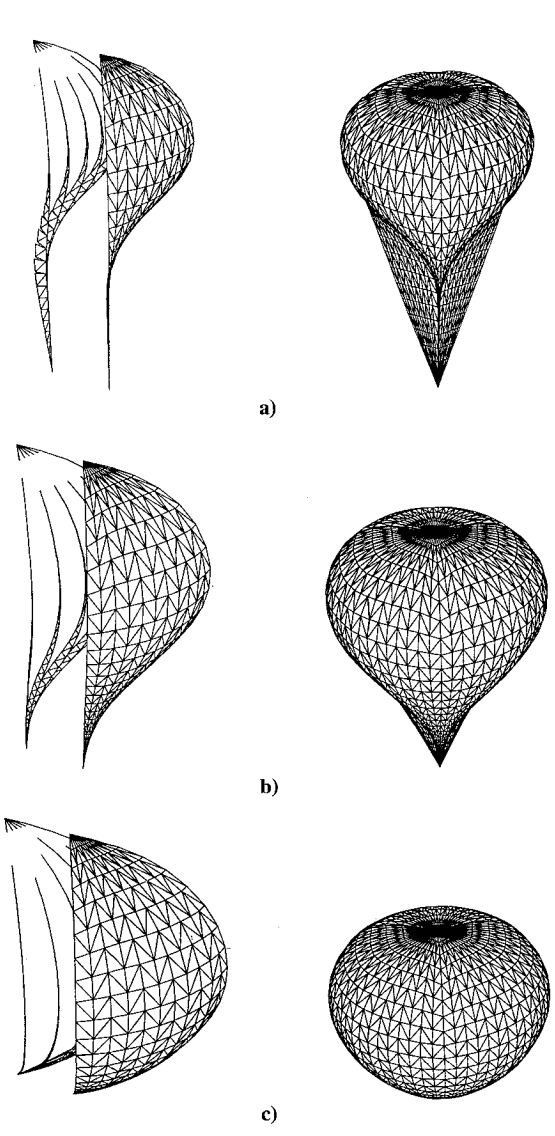

Fig. 6 Triangular symmetry—$\mathcal{S}_f$ (left) and $\mathcal{S}$ (right); a) $\mathcal{V} = 0.23 \cdot \mathcal{V}_{\text{float}}$, b) $\mathcal{V} = 0.53 \cdot \mathcal{V}_{\text{float}}$, and c) $\mathcal{V} = 0.87 \cdot \mathcal{V}_{\text{float}}$.

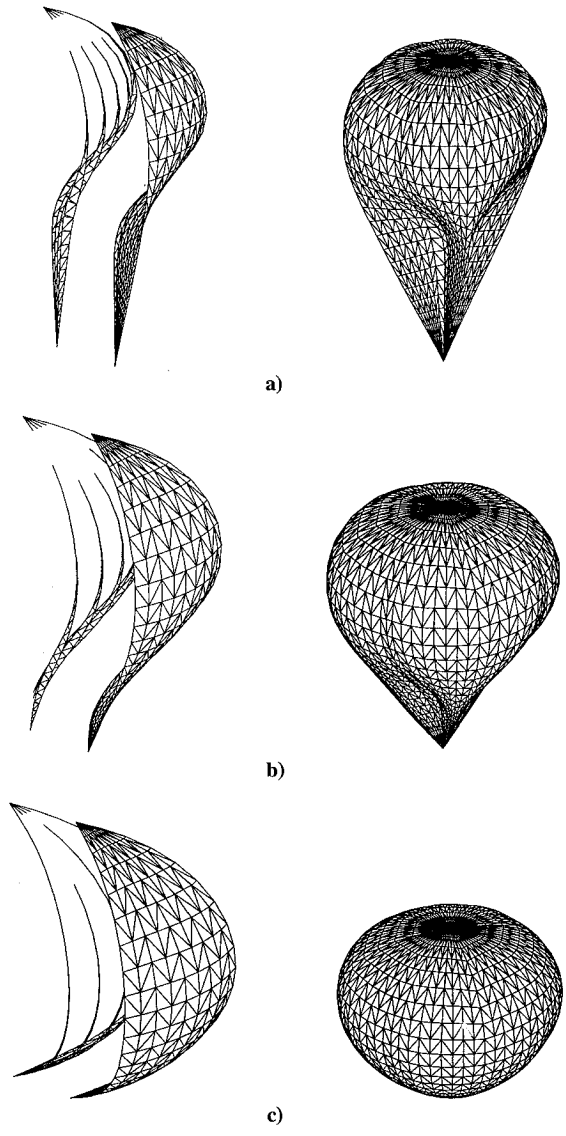

Fig. 7 Square-shaped symmetry—$\mathcal{S}_f$ (left) and $\mathcal{S}$ (right); a) $\mathcal{V} = 0.23 \cdot \mathcal{V}_{\text{float}}$, b) $\mathcal{V} = 0.53 \cdot \mathcal{V}_{\text{float}}$, and c) $\mathcal{V} = 0.87 \cdot \mathcal{V}_{\text{float}}$.

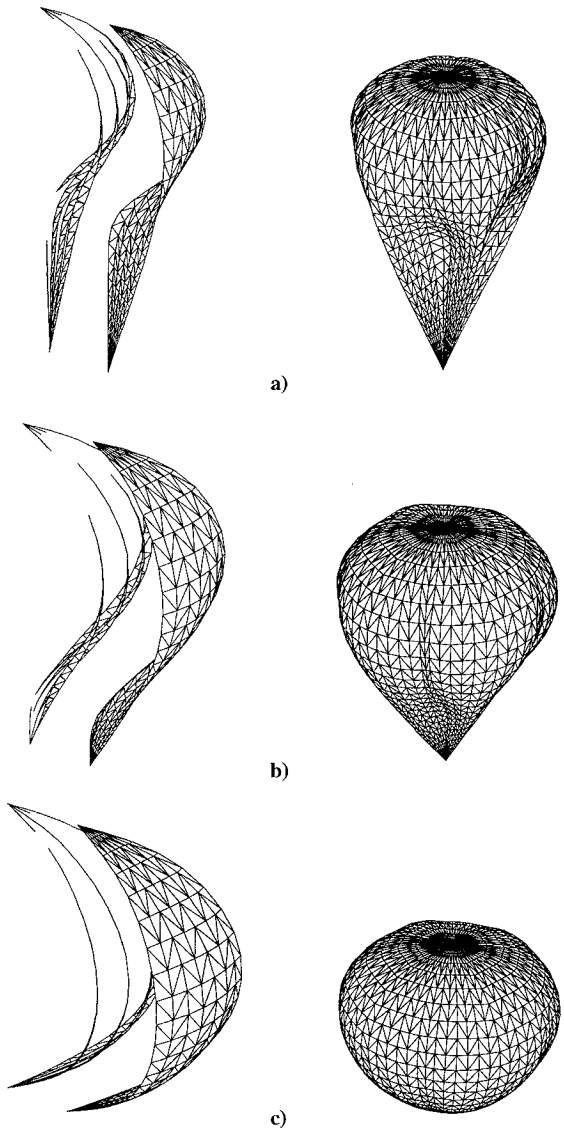

Fig. 8 Pentagonal symmetry—$\mathcal{S}_f^i$ (left) and $\mathcal{S}^i$ (right); a) $\mathcal{V} = 0.23 \cdot \mathcal{V}_{\text{float}}$, b) $\mathcal{V} = 0.53 \cdot \mathcal{V}_{\text{float}}$, and c) $\mathcal{V} = 0.87 \cdot \mathcal{V}_{\text{float}}$.

circumferential fiber, and $e_{d,l}$—a diagonal edge (see Figs. 4 and 5). In the following, $E_{m,l}$, $E_{c,l}$, and $E_{d,l}$ will denote the corresponding edges in $\mathcal{T}_l^R$ in the reference configuration.

For a shape in $\mathcal{C}_k$ to better match the geometry of a real ascent shape, we allow vertices along a meridional fiber to move—as long as their logical positions relative to their neighbors are preserved and the total length of the edges are equal to the L_m. Vertices and edges in the reference configuration are recomputed whenever a new $\mathcal{S}_f(v_{i,j})$ is specified. We will use the (relative) diagonal stretch

$$\frac{|e_{d,l}| - |E_{d,l}|}{|E_{d,l}|}$$

to measure the distortion in $\mathcal{T}_l$. Note that diagonal stretches can be positive or negative.

To gauge how well the constraints Eqs. (12–14) in Problem (⋆) are satisfied, we will consider their residuals. For this purpose, we define the following quantities:

$$\ell_{c,i} = |f_{i,1}| + d\left(v_{i,1}^M, v_{i,1}^R\right) + \sum_{j=2}^{p+1} d\left(v_{i,j}^L, v_{i,j}^R\right)$$

$$L_{c,i} = d\left(V_{i,1}^M, V_{i,1}^R\right) + \sum_{j=2}^{p+1} d\left(V_{i,j}^L, V_{i,k}^R\right)$$

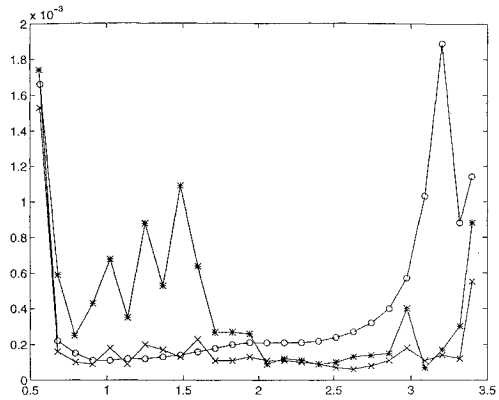

Fig. 9 Total meridional stretches—$(\mathcal{V}^i, \delta_{m,i}^{\pm})$, $i = 0, 1, \ldots, 25$; triangular symmetry (○), square-shaped symmetry (×), pentagonal symmetry (∗).

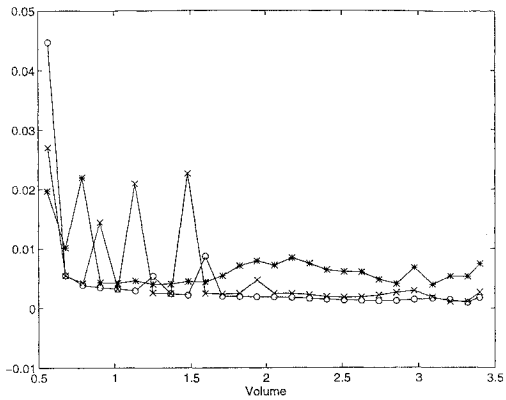

Fig. 10 Total circumferential stretches—$(\mathcal{V}^i, \delta_{c,i}^{\pm})$, $i = 0, 1, \ldots, 25$; triangular symmetry (○), square-shaped symmetry (×), pentagonal symmetry (∗).

$$\delta_c^+ = \max_{2 \le i \le n_c+1} \{(\ell_{c,i} - L_{c,i})/L_{c,i}\}$$

$$\ell_{m,j} = d\left(v_{1,2j}, v_{n_c+2,2j}\right)$$

$$L_m = d\left(V_{1,j}^R, V_{n_c+2,j}^R\right)$$

$$\delta_m^+ = \max_{1 \le j \le p+1} \{(\ell_{m,j} - L_m)/L_m\}$$

$$\delta_m^- = \min_{1 \le j \le p+1} \{(\ell_{m,j} - L_m)/L_m\}$$

Quantities such as δ_c^+ and $\delta_m^{\pm}$ measure the total stretch of circumferential and meridional fibers, respectively. By construction, $\ell_{c,i} \ge L_{c,i}$. For the EM families considered here, we found that $\delta_m^- > 0$ (that is, $\ell_{m,j} \ge L_m$ for all j). We define the maximum and minimum diagonal stretches for $\mathcal{S}_f(v_{i,j})$ as follows:

$$\delta_d^+ = \max\{(|e_{d,l}| - |E_{d,l}|)/|E_{d,l}|, \qquad l = 1, 2, \ldots, N_{\mathcal{T}}\}$$

$$\delta_d^- = \min\{(|e_{d,l}| - |E_{d,l}|)/|E_{d,l}|, \qquad l = 1, 2, \ldots, N_{\mathcal{T}}\}$$

respectively. We define the average diagonal stretches as

$$\hat{\delta}_d^+(\mathcal{S}) = \frac{1}{n\left(\mathcal{I}_d^+\right)} \sum_{l \in \mathcal{I}_d^+} (|e_{d,l}| - |E_{d,l}|)/|E_{d,l}|$$

$$\hat{\delta}_d^-(\mathcal{S}) = \frac{1}{n\left(\mathcal{I}_d^-\right)} \sum_{l \in \mathcal{I}_d^-} (|e_{d,l}| - |E_{d,l}|)/|E_{d,l}|$$

where $n(\mathcal{I})$ denotes the number of elements in $\mathcal{I}$ and

$$\mathcal{I}_d^+ = \{l \mid (|e_{d,l}| - |E_{d,l}|)/|E_{d,l}| > 0\}$$

$$\mathcal{I}_d^- = \{l \mid (|e_{d,l}| - |E_{d,l}|)/|E_{d,l}| < 0\}$$

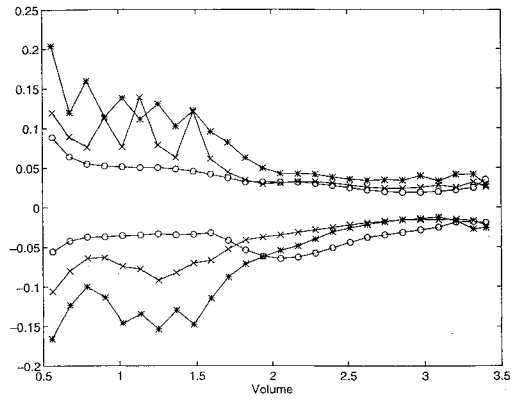

Fig. 11 Maximum and minimum diagonal stretches—$(\mathcal{V}^i, \delta^{\pm}_{d,i})$, $i = 0, 1, \ldots, 25$; triangular symmetry (○), square-shaped symmetry (×), pentagonal symmetry (∗).

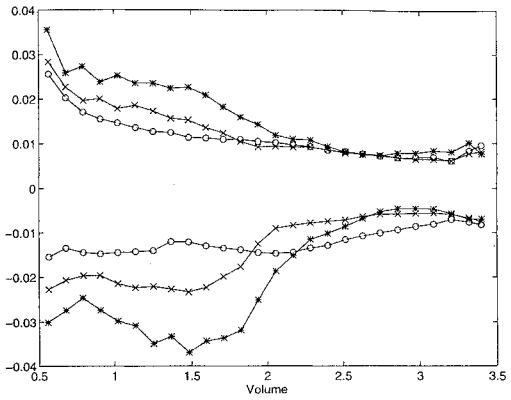

Fig. 12 Average diagonal stretches—$(\mathcal{V}^i, \hat{\delta}^{\pm}_{d,i})$, $i = 0, 1, \ldots, 25$; triangular symmetry (○), square-shaped symmetry (×), pentagonal symmetry (∗).

Since $\delta^{\pm}_d$ represent extreme values, they do not yield the best measure of the stretching that is present in the entire EM shape. Few triangles are distorted in the amounts $\delta^{\pm}_d$. For this reason, we use $\hat{\delta}^{\pm}_d$ as an overall measure of the distortion and $\delta^{\pm}_d$ as a measure of the maximum distortion in an EM shape.

We computed $\delta^{\pm}_m$, δ^{+}_c, $\delta^{\pm}_d$, and $\hat{\delta}^{\pm}_d$ for the three families of EM shapes presented in Sec. VI. In Fig. 9, we present plots of $(\mathcal{V}^i, \delta^{\pm}_{m,i})$, for $i = 0, 1, \ldots, 25$, for the triangular, square-shaped, and pentagonal families. Figure 10 contains plots of $(\mathcal{V}^i, \delta^{+}_{c,i})$, for $i = 0, 1, \ldots, 25$. Figure 11 contains plots of $(\mathcal{V}^i, \delta^{\pm}_{d,i})$, for $i = 0, 1, \ldots, 25$, and Fig. 12 contains plots of $(\mathcal{V}^i, \hat{\delta}^{\pm}_{d,i})$, for $i = 0, 1, \ldots, 25$.

VIII. Concluding Remarks

When we attempted to determine families of ascent shapes using the model in Ref. 2, we observed significant distortion in the computed EM shapes. Starting with $\mathcal{V} = 0.16 \cdot \mathcal{V}_{\text{float}}$, we were unable to converge to a solution satisfying all of the constraints for volumes greater than $0.33 \cdot \mathcal{V}_{\text{float}}$. However, with the introduction of the pseudogore structure and vertex averaging into our EM model, we are able to compute families of ascent shapes over a wide range of volumes—as low as 5% of $\mathcal{V}_{\text{float}}$ and as high as 100% of $\mathcal{V}_{\text{float}}$. By introducing a reference configuration, we can estimate the distortion in an EM shape. Table 1 summarizes the constraint residuals and distortion measures for the families of EM shapes that were presented in Sec. VII. When compared with EM shapes computed by the method in Ref. 2, we find that the local distortion in EM shapes computed by solving Problem (⋆) has been reduced significantly.

We found that the extreme values of $\delta^{\pm}_d$ were reduced by about 20%, if we carried out two iterations of Eqs. (16–18) instead of one in our vertex-averaging scheme (see Sec. V). The averaging scheme seemed to control the growth of δ^{+}_c, $\delta^{\pm}_m$, and $\delta^{\pm}_d$, when computing a family of ascent shapes. The values of the average diagonal stretches $\hat{\delta}^{\pm}_d$ did not change appreciably when the number of iterations was increased from one to two. Using a larger number of vertex-averaging iterations did not yield significantly better results.

The extreme values of $\delta^{\pm}_{d,i}$ occur for $i = 0$ in the pentagonal family of shapes, where $(\delta^{-}_{d,0}, \delta^{+}_{d,0}) = (-0.16562, 0.20386)$. It is important to keep in mind that these are the minimum and maximum values over all triangles in $\mathcal{S}^0_f$, and very few triangles are actually compressed/stretched in these amounts. In this example, we find that of a total of $N_{\mathcal{T}} = 322$ triangles, two diagonal edges are compressed in the amount of $\delta^{-}_{d,0}$ and two are stretched in the amount of $\delta^{+}_{d,0}$. If $\hat{\delta}^{\pm}_d$ are computed, we find that $(\hat{\delta}^{-}_{d,0}, \hat{\delta}^{+}_{d,0}) = (-0.03008, 0.03554)$. We say that the average diagonal stretches are about 4% in magnitude for this EM shape. This suggests the possibility of using an EM shape as the initial guess for a finite element method where a shape could be computed by minimizing a strain energy function.

The residuals for the total meridional fiber constraints are lower than those for the total circumferential fiber constraints. The difference is due to a tighter bound that is placed on the equality constraint Eq. (12). Initially, the meridional fibers are close to their target lengths and remain so through the evolution of an EM shape. Furthermore, inequality constraints are imposed on the circumferential fiber segments, so that it should not be surprising to find that circumferential fibers are stretched.

The Winker profile curves do not always provide a good initial guess for an EM shape. For a given fixed pair of profile curves with no circumferential stretching allowed, certain symmetries can be ruled out, because there may be insufficient material to form a complete circumferential fiber (see Ref. 3). However, in our current model, we allow circumferential fibers to stretch. The largest value of $\delta^{+}_{c,i}$ occurs for the D_3 shape at $i = 0$ where $\delta^{+}_{c,0} = 0.04470$. However, this is likely due to the poor initial guess that is used, since $\delta_{c,i} < 0.006$ for $i = 1, 2, \ldots, 25$. For the D_4 and D_5 cases, a number of spikes are observed in the values of $\delta^{+}_{c,i}$ for $i = 0, \ldots, 13$. Once again, these are most likely due to the errors introduced by using the initial guess based on the Winker profiles. These errors are inherited by $\mathcal{S}^i_f$ for $i \geq 1$ (even though their magnitudes decrease with increasing $\mathcal{V}$). Similar behavior is observed in $\delta^{\pm}_{m,i}$, except these increase in magnitude as the float volume is approached. Nevertheless, the values of $\delta^{\pm}_{m,i}$ are no more than 0.002. The diagonal stretches of the D_4 and D_5 shapes are initially much larger than those for the D_3 shape. However, after the volume exceeds 55% of $\mathcal{V}_{\text{float}}$ (i.e., $i = 12, \ldots, 25$), the values of $\delta^{\pm}_{d,i}$ are roughly the same for all three families of EM shapes. The magnitude of the quantities $\delta^{\pm}_{m,i}$, $\delta^{+}_{c,i}$, and $\delta^{\pm}_{d,i}$ can be reduced further by using a computed solution $\mathcal{S}^i_f$ as the initial guess for an evolution with target volume $\mathcal{V}^i$ (see Sec. 4.5 of Ref. 9 for a further discussion). This was done for $\mathcal{S}^{23}$ in the D_3 family (to reduce the size of $\delta^{+}_{m,23}$) and for $\mathcal{S}^{13}$ in the D_4 family (to reduce the size of $\delta^{+}_{c,13}$).

At float altitude, the Σ-shaped model with $\Sigma = 0.4$ predicts the maximum height of the balloon is $z_{\max} = 1.5912$ and its maximum radius is $r_{\max} = 1.0359$. In our EM model, the surface area $\mathcal{A}_{\text{float}}$ of the design shape depends on the total number of pseudogores but is roughly around 11.23. Because $\mathcal{A}_{\text{float}}$, $r_{\max}$, and $z_{\max}$ for our EM shapes are computed quantities and do not appear in constraint equations, we can compare these values to the corresponding design values to see how well our EM families evolve to the float shape. We found that the EM shapes are within 1% of the design values $\mathcal{A}_{\text{float}}$, $r_{\max}$, and $z_{\max}$ near float.

Unlike the standard Σ-shaped model whose solutions yield axisymmetric shapes, our EM shapes with pseudogores possess many of the large-scale nonaxisymmetric features that are observed in real balloons—a lobe pattern surrounding the gas bubble, internally folded material inside the gas bubble, and flat winglike structures below the gas bubble. In addition, the internal folds inside the gas bubble appear to initiate near the shoulder of the balloon for the ascent EM shapes (see $\mathcal{S}_f$ in Figs. 6–8). Since each pseudogore can store excess material, the EM-shaped model with pseudogores provides a good description of the internally folded material and is consistent with observations of partially inflated balloon shapes.

Acknowledgments

This research was supported by NASA Grant NAG5-697. The author would like to thank Bill Collier and Tami Williams for their assistance in carrying out part of the research presented in this paper.

References

[1]Anon., "Research Development in the Field of High Altitude Plastic Balloons," Univ. of Minnesota, Dept. of Physics, NONR-710(01) Repts., Minneapolis, MN, 1951–1956.

[2]Baginski, F., "A Variational Principle for Ascent Shapes of Large Scientific Balloons," 30th Scientific Assembly of COSPAR, PSB-003, Hamburg, July 1994.

[3]Baginski, F., and Ramamurti, S., "Variational Principles for Ascent Shapes of Large Scientific Balloons," *AIAA Journal*, Vol. 33, No. 4, 1995, pp. 764–768.

[4]Winker, J. A., "Stress Patterns, Shape Studies and Failure Analysis on Real Balloons," AIAA Paper 86-2518, Oct. 1986.

[5]Baginski, F., "Mathematical Modeling of Off-Design Balloon Shapes," 1992 NASA/ASEE Summer Faculty Fellowship Program Final Rept., NASA/GSFC/WFF Balloon Projects Branch, Wallops Island, VA, Aug. 1992.

[6]Brakke, K., "The Surface Evolver Manual," Version 1.91, The Geometry Center, Minneapolis, MN, May 1993.

[7]Powell, M. J. D., "A Fast Algorithm for Nonlinearly Constrained Optimization Calculations," *Numerical Analysis*, Vol. 630, edited by G. A. Watson, Lecture Notes in Mathematics, Springer–Verlag, New York, 1978.

[8]Morris, A. L. (ed.), "Scientific Ballooning Handbook," National Center for Atmospheric Research, NCAR-TN-99, Boulder, CO, 1975, Sec. V, pp. 1–45.

[9]Baginski, F., "Mathematical Modeling of Energy Minimizing Off-Design Shapes of Large Scientific Balloons II," Final Rept., NASA Grant NAG5-697, Jan. 1995.